

Microstructural characterization of API 5L X65 and X70 steels manufactured by TMCP process

Luan Mayk Tôrres Costa ^{1*} 

Gudson Nicolau de Melo ¹

Nicolau Apoena Castro ¹

Augusto José de Almeida Buschinelli ¹

Abstract

This work shows the microstructural characterization of API-5L X65 and X70 steels manufactured by the TMCP process. Images are obtained by optical microscopy (OM), scanning electron microscopy (FEG-SEM) and atomic force microscopy (AFM). Besides, the EBSD technique pointed out that both samples are presenting a refined quasi-polygonal ferrite matrix with eutectoid aggregates in the contours and vertices of ferritic grains. Moreover, a grain size of 8.4 μm is estimated for X70 and 10.6 μm for X65 steel. In the AFM images, eutectoid aggregates displayed higher relief concerning the ferrite matrix, and these microconstituents' higher hardness causes them. This behavior is in agreement with the results of the Vickers Hardness test. EBSD showed that the quantity of microphases in the X65 is slightly higher than in the X70. However, the X70 steel presented higher high and low angle lengths due to the greater refinement and stronger cooling rates applied during processing. The Vickers test showed that the ferrite hardness is similar for both steels. This same behavior is verified for the Vickers test in eutectoid aggregates. It indicates that the higher strength of X70 sample is mainly a consequence of the finer microstructure.

Keywords: API; Scanning electron microscopy; Atomic Force Microscopy; EBSD.

1 Introduction

The growth in global energy demand is increasingly requiring the production and consumption of oil products [1]. The use of pipes are the most efficient method of transporting these fluids in combining economic viability, safety, reliability, regularity and efficiency. In search of higher productivity in the transmission lines, it became necessary to employ adequate materials that guarantee greater security and reduced cost [2,3]. HSLA (High-Strength Low-Alloy) steels are used for pipe manufacturing process because of their high mechanical strength, good toughness in low temperature and hydrogen embrittlement resistance [4-6], as well as the corrosion resistance. The latter is required due to the corrosion risk caused by the chemical composition of the transported fluids [7,8]. By virtue of these characteristics, these steels enable the transmission line to withstand the same given working pressure with reduced wall thickness, reducing the pipe weight, increasing the pipeline output and ensuring economy [3,9]. These steels consist of micro-alloyed materials which have a typical chemical composition based on Fe, C, Mn, Nb, Ti and V, and may also have residual contents of other elements. The classification is given by the American Petroleum Institute through the API-5L -

Specification for line pipe steel, and the specification sets the minimum flow limit [10].

The demand for more efficient working conditions and the implementation of pipes in extreme conditions [11] have leveraged the development of more advanced production methods [2,12]. Until the late 1960s, their production was by hot rolling followed by normalizing [13]. In this process, the steel produced has the microstructure that is formed by polygonal ferrite and perlite. It requires the use of higher carbon contents and alloying elements to increase the mechanical strength, which in turn reduces the weldability and the product toughness. The development of the controlled rolling i-e Thermo-mechanical Controlled Rolling (TMCR), through the thermo-mechanical treatment with the addition of micro-alloying such as niobium, titanium and vanadium promoted a more refined microstructure, is formed by a ferritic matrix with a second predominantly perlitic constituent, thus enabling to reduce the carbon. The main step of the TMCR process is to perform successive hot rolling passes that is in a temperature range, in which no austenite recrystallization occurs. Thus, ensuring austenite-ferrite transformation is in the hardened state. Thereby obtaining greater microstructural

¹Universidade Federal do Rio Grande do Norte, UFRN, Natal, RN, Brasil.

*Corresponding author: luanmayk.ufrn@gmail.com



refinement, higher mechanical strength thus lowering weldability and toughness compromises [9,13,14].

The processing of these steels had been undergone through a significant advancement in the early 1980s with the emergence of TMCP. The application of accelerated cooling after the rolling steps ensures greater microstructural refinement, lower carbon and alloying contents, and an excellent combination of mechanical strength, toughness and weldability as a result of the refined microstructure formed by low temperature ferritic constituents and different types of bainite [15-17]. This enable manufacturing higher API grade steels, which guarantees a reduction in pipe thickness in addition to the aforementioned properties [18,19], reduction in welding passes and lower plate reheat temperature [15].

Different constituents can be found in API steels according to the chemical composition, cooling rate, initial and final cooling temperature, etc. This variation, as well as the combination of distinct morphologies and phases, strongly influences the mechanical properties of the manufactured pipes. Different types of ferrite (acicular, polygonal, quasi-polygonal), bainite (granular, superior and inferior), perlite and martensite-austenite (MA) microconstituent are the most commonly found microstructures [12,14,20].

The TMCP characteristics lead to manufacturing products with more complex microstructures and high refinement.

As this process has been applied abundantly, the development of a microstructural study is essential to better understand the process, seeking to improve the performance of these steels.

The formed constituents and phases have a morphology that is difficult to identify only by conventional analysis (such as MO and SEM), showing the importance of using several techniques simultaneously, such as AFM, EBSD.

The main purpose of this paper is to study the steels microstructure relating them to their mechanical properties and to the TMCP process. Different microscopic techniques are applied to study the higher strength of X70 sample through the microstructure differences. AFM images are used to give more information about the MA microconstituent in a 3D-scale.

2 Materials and methods

In this work, an effort is made to characterize two API steels, X65 and X70, produced on a pilot scale through controlled rolling followed by accelerated cooling, at the Usiminas SA Research Center. The main difference between two steel processing is the cooling rate after finishing rolling.

The X70 steel has been processed with a cooling rate almost three times higher than the X65. The chemical composition is given in Table 1.

Samples has been taken from the cross-sections of the rolling direction. They are prepared by sanding and polishing. After that, etched with 2% Nital solution. After preparation, the samples are analyzed by optical microscopy (Nikon Microscope - Model: Eclipse MA 200), field emission gun scanning electron microscopy (Zeiss Auriga 40) and atomic force microscopy (Shimadzu SPM-9700) in the intermittent contact mode.

For the electron backscatter diffraction (EBSD) evaluation, the samples have been prepared by sanding, polishing with diamond paste and finished by an ultrafine polishing with colloidal silica. Images are performed using a Bruker E-Flash 1000 detector, using a 0.23 μm step. The results are processed in the Bruker Esprit version 2.1 software. IQ (Image Quality) maps, high angle (HAC) and low angle (LAC) contours, average grain sizes, percentages of microphases and total lengths of the contours are obtained. The following condition has been considered for critical orientation differences to identify the contours (θ): LAC: $2^\circ < \theta < 15^\circ$; HAC: $\theta > 15^\circ$. It is considered the sum of the austenite, cementite and low IQ points for quantifying eutectoid aggregates. This sum of regions tends to have low quality indices due to the high dislocation density present in microconstituents transformed at low temperatures. All points with IQ lower than 0.42 are considered as eutectoid aggregates. This critical value has chosen through the qualitative evaluation of the IQ histogram.

Vickers microhardness is applied to estimate both the ferritic matrix and the eutectoid microconstituents hardness. Ten indentations are performed for each constituent, with 5 gf loading applied for 10 seconds.

3 Results and discussion

3.1 Optical Microscopy (OM)

General aspects of the microstructure are evaluated by OM. Figure 1 shows some micrographs of the X65 and X70 samples etched by 2% Nital reagent. The strengthening mechanisms through solid solution, phase transformation, precipitation and work hardening contribute to the higher yield strength in steels. However, grain refinement is the main mechanism for a higher grade API steels, as it is the only mechanism that simultaneously increases both mechanical strength and toughness without compromising weldability.

Table 1. Chemical composition of the X65 and X70 steels. The contents of carbon is measured by Optical Emission Spectroscopy while the rest is obtained by X-ray fluorescence (mass fraction wt. %)

Sample	C	Mn	Si	Ti +Nb + V	Ni +Cu +Mo
X65	0.03	1.17	0.26	< 0.15	< 0.5
X70	0.04	1.35	0.27	< 0.15	< 0.5

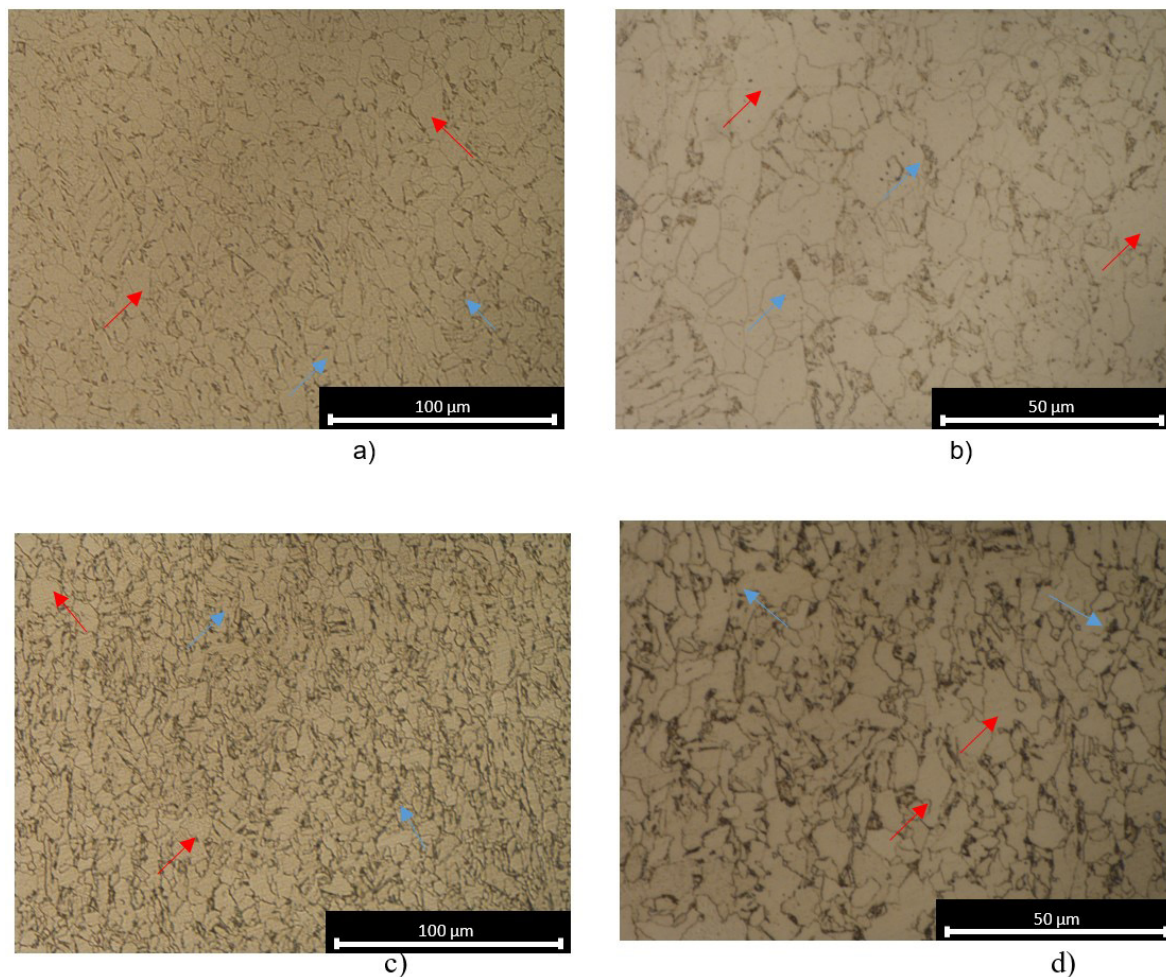


Figure 1. OM micrographs etched by 2% Nital reagent. a) X65 steel image with original magnification of 500X; b) X65 steel image with original magnification of 1000X; c) X70 steel image with original magnification of 500X; d) X70 steel image with original 1000X magnification. Red arrows indicate quasi-polygonal ferritic structure and blue arrows indicate eutectoid aggregates.

A finer grain presents higher grain boundary volume, which is obstacle to the dislocation movement. For this reason, the quantity of alloying elements is reduced [14,19,20].

It can be observed that although it is not measured quantitatively, there is a tendency for greater microstructural refinement in the X70 steel. The X65 and X70 steels have similar microstructures, presenting both a quasi-polygonal ferrite matrix (light regions of Figure 1 a), b), c) and d) - red arrow) with eutectoid aggregates (dark regions - blue arrow). The low magnification provided by OM does not allow to define the type of eutectoid aggregate found, for which higher resolution powers are required.

3.2 Field Emission Gun Scanning Electron Microscopy (FEG-SEM)

FEG-SEM images are showed in Figure 2. The Figures a) and c), respectively, show the formation of quasi-polygonal ferrite and some higher aspect ratio (more elongated) ferritic grains, similar to acicular ferrite.

The occurrence of eutectoid aggregates is also verified, characterized as MA microconstituent (blue arrows), and preferentially located in the grain boundaries and at the interface of three or more grains. In Figure 2b), there is a region composed of quasi-polygonal ferrite, with MA microconstituent and carbide precipitation (yellow ellipse). The behaviors already mentioned are observed in d), e) and f), and the white arrow in the latter points to the formation of eutectoid aggregates, which are difficult to be characterized even at considerably high magnifications. Regarding the images obtained via OM, it can be verified via SEM-FEG that the X70 steel sample has greater microstructural refinement.

The MA microconstituent consists of retained austenite islands with martensite slats. There are difficulties in its characterization via SEM, since it is not possible to identify the retained austenite present between the martensitic needles, which can be done via transmission electron microscopy (TEM) [21]. However, the results obtained in this work show a good resemblance to the content presented by Bott et al. [22], which describe morphological aspects (via

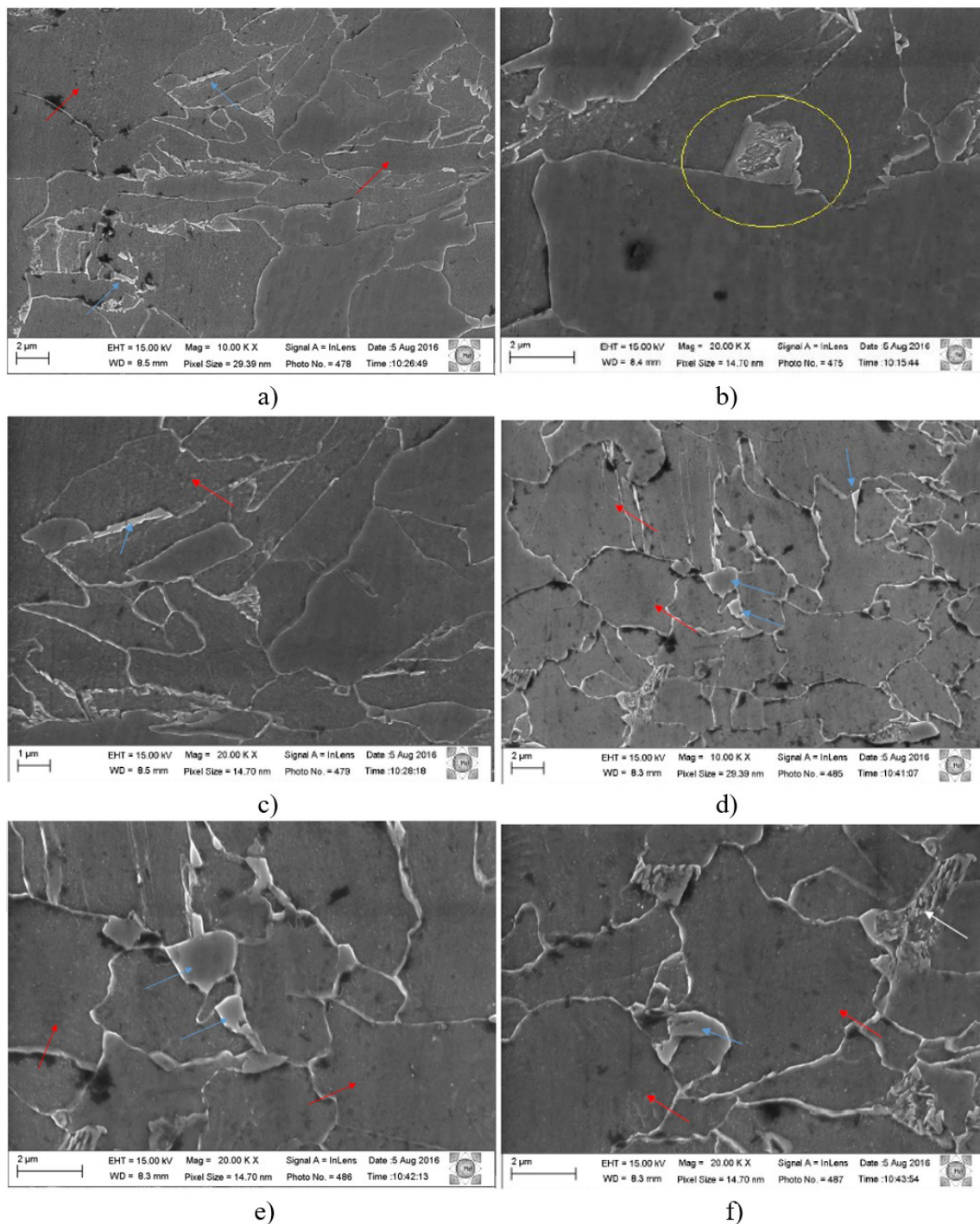


Figure 2. FEG-SEM images of samples etched with 2% Nital solution. a) X65 steel with original magnification of 10000X; b) and c) X65 steel with original magnification of 20000X; d) X70 steel with original magnification of 10000X; e) and f) X70 steel with original magnification of 20000X. Red arrows indicate possible quasi-polygonal ferritic structure formation, blue and white arrows indicate eutectoid aggregates, and yellow ellipse points to possible precipitation of carbonates.

SEM) of ferrite and MA microconstituent in API Nb-Cr-Mo microalloyed steels. The morphological characteristics of the MA constituent are in agreement with the aspects presented by Bonnevie et al. [23] in their study via OM with Picral solution.

3.3 Atomic Force Microscopy (AFM)

The study of eutectoid aggregates from heat treatments via continuous cooling is often complex, requiring high resolution techniques, such as Transmission Electron

Microscopy [21] and Atomic Force Microscopy. The AFM analysis is performed in order to complete the microstructural study of the X65 and X70 steels, mainly to give more details of the eutectoid aggregates. The acquired topography maps are shown in Figures 3 to 5.

The images acquired via AFM correspond to the topographic mapping of the selected area, assigning a color scale to the values obtained. According to the scales shown in the Figures 3 a) and b), the low relief corresponds to dark tones, while the high relief corresponds to light tones. The

topography presented in the samples originated from polishing and metallographic etching. As ferrite is a soft phase and more susceptible to chemical etching with Nital reagent, it is expected that the ferritic regions are in low relief, while the aggregates are in high relief. This difference of relief is in consequence of the interaction forces between the AFM probe and the steel phases.

As discussed above, the distinct behavior between ferritic grains and eutectoid aggregates provided high contrast AFM imaging, enabling differentiation between

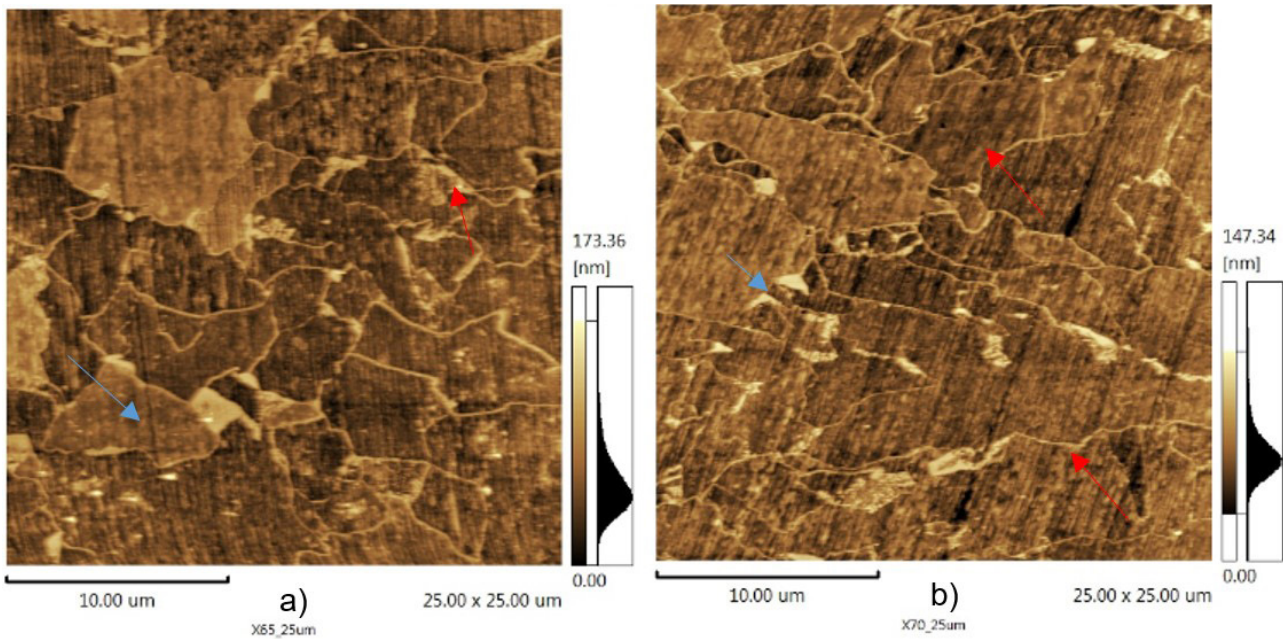


Figure 3. Images via AFM in an area of 25 μm x 25μm. The color scale represents the topographic levels of the analyzed surfaces. a) X65 Steel; b) X70 Steel.

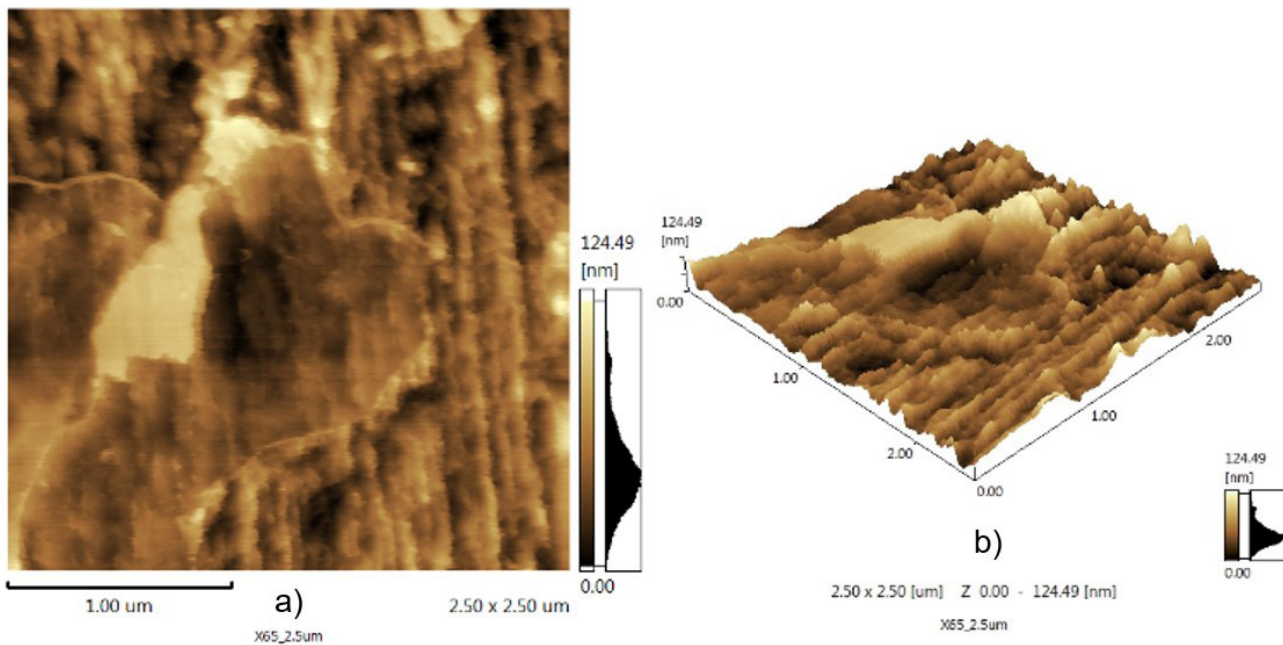


Figure 4. Image via AFM in an area of 25 μm x 25 μm of X65 steel. a) topographic map; b) three-dimensional map of the surface.

ferrite and aggregates. The latter can be seen in high relief (light regions), while ferrite appears in low relief, consisting of darker and less hard regions.

As observed by SEM, AFM images enabled identifying aggregates smaller than 1 μm diameter, located in ferritic grain boundaries. It is also noted that these aggregates can have varied shapes. Figure 4a shows aggregates with a lower aspect ratio, while in others regions they are found with longer shape (ellipses highlighted in Figure 5a). The aspects of the aggregates characterized by FEG-SEM and through the AFM maps (which showed the presence of regions with high hardness) are compatible with the MA microconstituent.

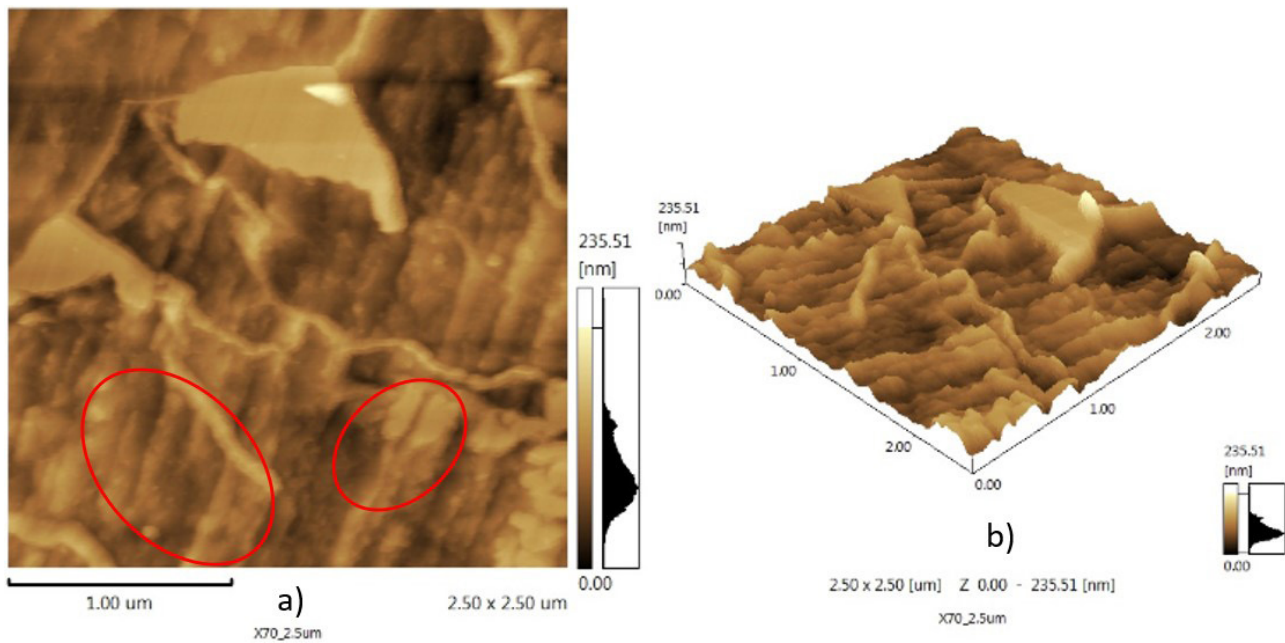


Figure 5. Image via AFM in an area of 25 μm x 25 μm of X70 steel. a) topographic map; b) three-dimensional map of the surface.

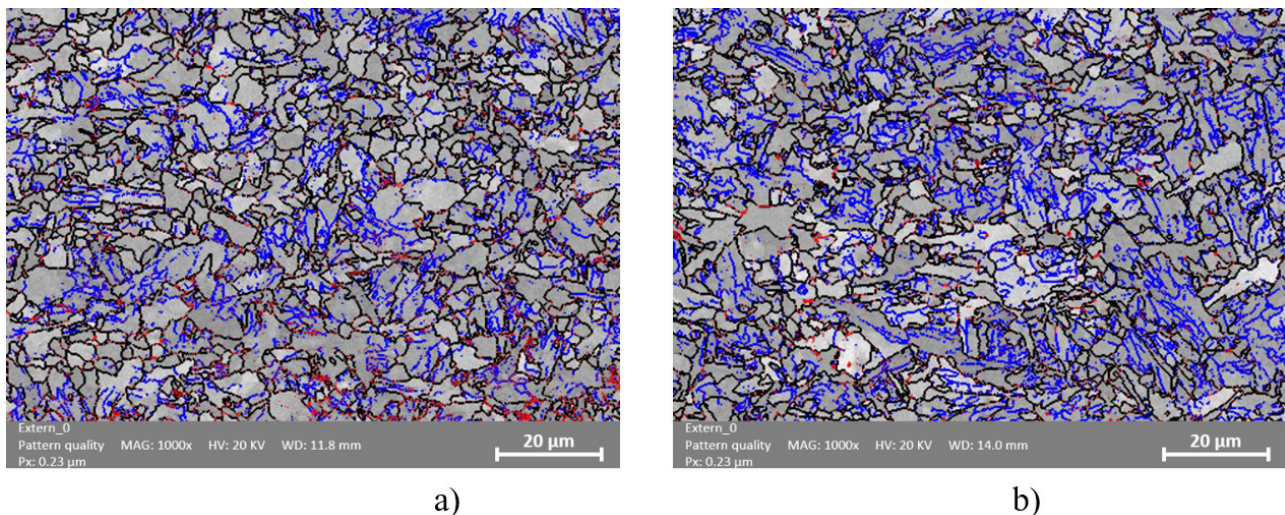


Figure 6. Images obtained from EBSD containing IQ maps, grain boundaries and eutectoid aggregates. a) X65; b) X70. HAC and LAC are presented in black and blue, respectively. The eutectoid aggregates regions are in showed in red.

3.4 Electron Backscatter Diffraction (EBSD)

IQ maps, high and low angle contours (HAC and LAC) and eutectoid aggregates of X65 and X70 steels are shown in Figure 6. HAC and LAC are indicated in black and blue, respectively while the aggregates are in red. Figure 7 shows the IQ histograms obtained by EBSD analysis, from which the critical value for quantification of eutectoid aggregates is obtained qualitatively.

Figure 7 shows that the histograms obtained do not present any distortion in relation to the normal distribution, with a slight left shift. This behavior is a result of the eutectoid aggregates presence, which contain a high dislocation density

due to their lower transformation temperatures. Results in greater distortion of the backscattered electron diffraction pattern and consequently, lower IQ values. After analysis of the histogram, it is considered that regions with an IQ lower than 0.42 are eutectoid aggregates.

Quantitative parameters are measured via EBSD to complete the qualitative results already indicated. The determination of the average grain size, eutectoid aggregate fraction and high and low angle contour length are obtained using the Bruker Esprit 2.1 software. The results are presented in Table 2.

As expected, the X70 steel has presented a smaller average grain size (8.4 μm) than the X65 (10.6 μm). In addition, the overall contour lengths, especially those at low angles, are longer for the X70 steel as a result of the smaller grain size and higher cooling rates applied to this material.

Therefore, it is evident that the steel with higher yield strength (API X70) presented a more refined microstructure. This follows the law presented by Hall-Petch, indicating that a smaller average grain size implies a larger grain boundary area, reducing the dislocation mobility, increasing

the shear stress and, consequently, the yield strength steel. In addition, the longer low angle contour length for X70 steel also contributes to the increased yield strength. This behavior is because of the higher cooling rate to which this material has been subjected. The percentage of eutectoid aggregate is slightly higher in the X65 steel. It indicates that the stronger cooling rate in the X70 has not increased the quantity of these constituents.

3.5 Vickers microhardness

The Vickers microhardness test values are given in Table 3. As expected, ferritic grains presented lower hardness than eutectoid aggregates, as they are softer. The average hardness of the ferrite is similar in both steels. The same happened with the aggregates, pointing out that there is no significant variation in phase hardness between the samples. This means that the hardness of the phases is similar in the two API classes. Analyzing the results showed in Table 3, it can be deduced that the higher strength in the X70 sample does not derive from a difference in the phase hardness.

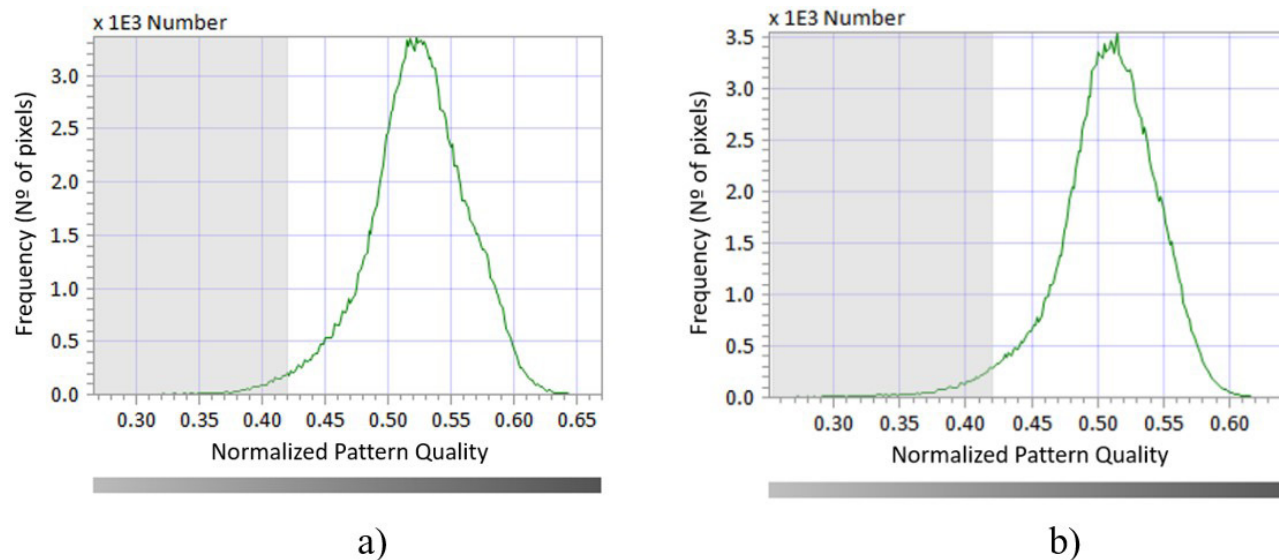


Figure 7. IQ histograms obtained via EBSD of X65 a) and X70 b) steel samples. The normalized distribution of the pattern quality is given by the number of pixels.

Table 2. Comparative EBSD results of the X65 and X70 steels: percentage of eutectoid aggregates, average grain size and lengths of HAC and LAC

EBSD Analysis Results							
API 5L-X65				API 5L-X70			
Average grain size (μm)	% of eutectoid aggregates	Length of HAC (μm)	Length of LAC (μm)	Average grain size (μm)	% of eutectoid aggregates	Length of HAC (μm)	Length of LAC (μm)
10.6 ± 0.7	4.8 ± 0.5	10.2 ± 0.2	4.0 ± 0.2	8.4 ± 0.6	4.2 ± 0.5	11.7 ± 0.7	5.3 ± 0.7

Table 3. Vickers microhardness test of the ferritic and eutectoid aggregates phases present in both X65 and X70 steels – load: 5gf

Vickers microhardness analysis – load: 5gf			
API 5L-X65		API 5L-X70	
Ferritic grain (HV)	Eutectoid aggregates (HV)	Ferritic grain (HV)	Eutectoid aggregates (HV)
145 ± 3	202 ± 4	143 ± 11	206 ± 5

Smaller average grain size is probably the mainly reason of the greater strength.

4 Conclusion

Both steels presented have similar microstructure: refined, with typically quasi-polygonal ferritic matrix and eutectoid aggregate islands of different morphologies. Some areas with acicular ferrite have been detected. By OM and MEV-FEG, the aggregates nucleated, preferably, in the boundaries and vertices of the ferritic grains. These latter presented quite varied aspects: some regions with a low aspect ratio, and longer shapes in others.

The AFM images have entrenched the results already obtained via OM and FEG-SEM. In addition, they promote a surface topographic study. While regions with eutectoid aggregates are presented in a high relief, constituting a result compatible with the high hardness of these constituents, the ferrite is found in low relief.

The Vickers microhardness test shows that the hardness of the ferrite and eutectoid aggregate is the same in both of the studied steels. The ferritic matrix and second phase, described by the aggregates, have the same values statistically, regardless of the increase of the API class.

Finally, from the EBSD quantitative study, the X70 has presented smaller average grain size and longer low and high angle contour lengths compared to the X65, contributing to the increase the mechanical strength of the material. The X65 has formed around 10% more MA constituent than the X70.

Acknowledgements

The authors thank the following Brazilian research financing institutions for support: The ANP and FINEP, for financial support. The Usiminas SA, for supplying the samples. The CAPES and PPGCEM-UFRN, for the experimental procedure.

References

- 1 Agência Nacional do Petróleo, Gás Natural e Biocombustíveis. Natural gas and biofuels statistical yearbook 2019. Rio de Janeiro: ANP; 2019.
- 2 Green KP, Jackson T. Safety in the transportation of oil and gas: pipelines or rail? *Fraser Research Bulletin*. 2015;1-14.
- 3 Hansen ME, Dursteler E. Pipeline, rail & trucks: economic, environmental, and safety impacts of transporting oil and gas in the U.S. USA: Strata; 2017.
- 4 Arora KS, Pandu SR, Shajan N, Pathak P, Shome M. Microstructure and impact toughness of reheated coarse grain heat affected zones of API X65 and API X80 linepipe steels. *International Journal of Pressure Vessels and Piping*. 2018;163:36-44.
- 5 Jorge LJ, Cândido VS, Silva ACR, Garcia FC Fo, Pereira AC, Luz FS, et al. Mechanical properties and microstructure of SMAW welded and thermally treated HSLA-80 steel. *Journal of Materials Research and Technology*. 2018;7(4):598-605.
- 6 Mohammadjoo M, Valloton J, Collins L, Henein H, Ivey DG. Characterization of martensite-austenite constituents and micro-hardness in intercritical reheated and coarse-grained heat affected zones of API X70 HSLA steel. *Materials Characterization*. 2018;142:321-331.
- 7 Montes OF, Garcés RS, Reyes RFA, Robledo PCZ, López FHE, Calderón FA. Comportamiento a la corrosión del acero API X70 soldado por el proceso de doble arco sumergido inmerso en diferentes medios corrosivos. *Soldagem e Inspeção*. 2016;21(2):172-184.
- 8 Biezma MV, Andrés MA, Agudo D, Briz E. Most fatal oil & gas pipeline accidents through history: a lessons learned approach. *Pipelines & Corrosion & Risk Failure Analysis*. 2020;110:104446.
- 9 Hillenbrand H, Kalwa C. High strength line pipe for project cost reduction. *World pipelines*. 2002;2(1):11.
- 10 American Petroleum Institute. Specification for line pipe – API specification 5L. 42nd ed. Washington: API; 2000.
- 11 Zakharova M. Risk analysis of accidents in reservoirs and gas pipelines for conditions in the arctic. *Procedia Structural Integrity*. 2019;20:108-112.
- 12 Rosado DB, Waele WD, Vanderschueren D, Hertelé S. Latest developments in mechanical properties and metallurgical features of high strength line pipe steels. *Sustainable Construction and Design*. 2013;4(1):1-10.
- 13 Hillenbrand HG, Gras M, Kalwa C. Development and production of high strength pipeline steels. In: *Proceedings of the International Symposium Niobium*; 2001; Orlando, USA. Orlando, Florida: Editora Europipe.

- 14 Grimpe F, Meimeth S, Heckmann CJ, Liessem A, Gehrke et al. Development, production and application of heavy plates in grades up to X120. In: Proceedings of the 1st International Conference on Super-High Strength Steels; 2005; Rome. Rome: Associazione Italiana di Metalurgia/Centro Sperimentali Materiali; 2005. p. 10.
- 15 Turani LO. A Tecnologia CLC de produção de chapas grossas aplicada à Indústria de Petróleo e Gás. In: Anais do II Seminário de Óleo, Gás e Energias Renováveis; 2010; Ipatinga, MG. Ipatinga, MG, Brazil: Editora Usiminas SA; 2010.
- 16 Mandal G, Ghosh SK, Chatterjee S. Effects of TMCP and QT on microstructure and properties of ultrahigh strength steel. *Materials Today: Proceedings*. 2019;18:5196-5201.
- 17 El-Shenawy E, Reda R. Optimization of TMCP strategy for microstructure refinement and flow-productivity characteristics enhancement of low carbon steel. *J Mater Res Technol*. 2019;8(3):2819-2831.
- 18 Igi S, Sakimoto T, Endo S. Effect of internal pressure on tensile strain capacity of X80 pipeline. *Procedia Engineering*. 2011;10:1451-1456.
- 19 Hillenbrand HG, Liessem A, Biermann K, Heckmann CJ, Schwinn V. Development of grade X120 pipe material for high - pressure gas transportation lines. In: Proceedings of the 4th International Conference on Pipeline Technology; 2004; UK. Beaconsfield, UK : Scientific Surveys Ltd.; 2004. p. 823-836.
- 20 Sohn SS, Han SY, Shin SY, Bae JH, Lee S. Analysis and estimation of the yield strength of API X70 and X80 linepipe steels by double-cycle simulation tests. *Metals and Materials International*. 2013;19:377-388.
- 21 Wang, C; Wu, X; Liu, J; Ning X. Transmission electron microscopy of martensite/austenite islands in pipeline steel X70. *Materials Science and Engineering*. 2006;438-440:267-271.
- 22 Bott IDS, De Souza LFG, Teixeira JCG, Rios PR. High-strength steel development for pipelines: A Brazilian perspective. *Metallurgical and Materials Transactions A: Physical Metallurgy and Materials Science*. 2005;36(2):443-454.
- 23 Bonnevie E, Ferrière G, Ikhlef A, Kaplan D, Orain J. Morphological aspects of martensite-austenite constituents in intercritical and coarse grain heat affected zones of structural steels. *Materials Science and Engineering*. 2004;385;1-2:352-335.

Received: 02 Dec. 2020

Accepted: 24 Sep. 2021